J. Fluid Mech. (2002), *vol.* 455, *pp.* 387–411. © 2002 Cambridge University Press
DOI: 10.1017/S0022112001007558 Printed in the United Kingdom

Steady-state chimneys in a mushy layer

By C. A. CHUNG† AND M. GRAE WORSTER

Institute of Theoretical Geophysics, Department of Applied Mathematics and Theoretical Physics, University of Cambridge, Silver Street, Cambridge CB3 9EW, UK

(Received 12 February 2001 and in revised form 23 October 2001)

Motivated by industrial and geophysical solidification problems such as segregation in metallic castings and brine expulsion from growing sea ice, we present and solve a model for steady convection in a two-dimensional mushy layer of a binary mixture. At sufficiently large amplitudes of convection, steady states are found in which plumes emanate from vertical chimneys (channels of zero solid fraction) in the mushy layer. The mush–liquid interface, including the chimney wall, is a free boundary whose shape and location we determine using local equilibrium conditions. We map out the changing structure of the system as the Rayleigh number varies, and compute various measures of the amplitude of convection including the flux of solute out of the mushy layer, through chimneys. We find that there are no steady states if the Rayleigh number is less than a global critical value, which is less than the linear critical value for convection to occur. At larger values of the Rayleigh number we find, in agreement with experiments, that the width of chimneys and the height of the mushy layer both decrease relative to the thermal-diffusion length, which is the scale height of the mushy layer in the absence of convection. We find evidence to suggest that the spacing between neighbouring chimneys at high Rayleigh numbers is smaller than the critical wavelengths of both the linear and global stability modes.

1. Introduction

When binary mixtures are directionally solidified, a mushy layer comprising a solid matrix of crystals with interstitial liquid commonly forms between the melt and solid regions (Copley *et al.* 1970). These mushy layers are the result of a supercooling-induced morphological instability of the solidification front (Mullins & Sekerka 1964). An introduction to mushy layers is given in Worster (2000), while a more comprehensive review of convection within them can be found in Worster (1997).

Of particular interest is the formation of 'chimneys', which are narrow, solid-free, cylindrical regions that form within the mushy layer as a result of convection. They can form when a mixture is cooled from below and the interstitial liquid is buoyant, or when a mixture is cooled from above and the residual liquid is relatively dense. In each case, the compositional buoyancy causes the residual liquid to convect from cooler to warmer regions of the mushy layer. Because the fluid can equilibrate its temperature to its new environment quickly, owing to thermal diffusion, but is relatively depleted of the slower-diffusing solute, it dissolves the surrounding solid to maintain its thermodynamic equilibrium. This process increases the permeability locally, enhances the flow out of the mushy layer, and finally focuses the fluid into a narrow, solid-free, vertical chimney.

† Present address: Department of Mechanical Engineering, National Central University, Chung-li, Taiwan 32054.

https://doi.org/10.1017/S0022112001007558 Published online by Cambridge University Press

In industrial settings, chimneys are highly undesirable because they result in local variations of the composition and microstructure of the casting, seen as 'freckle' defects (Sample & Hellawell 1984). Chimneys are also known to occur within sea ice (Eide & Martin 1975; Wettlaufer, Worster & Huppert 2000), and they may form within some magma chambers (Tait & Jaupart 1992; Jellinek & Kerr 2001) and at the Earth's inner–outer core boundary (Fearn, Loper & Roberts 1981; but see Bergman & Fearn 1994). In these geophysical settings, predictions of the fluxes through chimneys will be essential in determining the strengths of the driving mechanisms for the circulation of the oceans and the geodynamo.

Some previous numerical computations of convection in mushy layers have been conducted based on a single Darcy–Brinkman formulation for the combined mushy, liquid and chimney regions (for example, Felicelli, Heinrich & Poirier 1991 and Schneider *et al.* 1997). Though chimneys have been found in these studies, they have not been highly resolved numerically.

An alternative approach is to concentrate on steady-state systems and to treat the mushy and liquid regions in separate domains. The fluid motion within the mushy region is modelled by Darcy's equation, while that in the liquid region is modelled in general by the Navier–Stokes equations. It is then necessary to match the thermodynamic and fluid-mechanical variables across the mush–liquid interfaces, the positions of which also need to be determined as part of the overall solution. Moreover, the chimney wall is itself a free boundary, which must be determined.

Roberts & Loper (1983) used lubrication theory to model the flow through a chimney of prescribed uniform cross-section and analysed some aspects of the flow in the mushy layer around the chimney. Worster (1991) used a scaling analysis to elucidate the boundary-layer structure around a chimney, the principal features of which were later confirmed by a numerical analysis conducted by Schulze & Worster (1998). Their numerical model, which was two-dimensional, introduced aspects of the free-boundary nature of the problem by allowing the chimney wall and the top mush–liquid interface to adjust to the flow and temperature fields, though these interfaces were both assumed to be planar. Loper & Roberts (2001) present an asymptotic analysis in which the chimney walls are vertical to leading order and the width of the chimney is determined from a condition applied at its vent.

Schulze & Worster (1999), in extending previous weakly nonlinear analyses (Amberg & Homsy 1993; Anderson & Worster 1995; Chung & Chen 2000*a*) numerically, discovered that the development of steady-state convection leads to the suggestion of a region of negative solid fraction in the interior of the mushy layer. Such a region actually becomes a liquid inclusion. Thus a new, interior mush–liquid interface is created. Schulze & Worster discovered that the boundary conditions previously applied at mush–liquid interfaces are no longer independent, and hence are insufficient to close the problem uniquely, when there is fluid flow from mush to liquid, as at the base of a liquid inclusion. They derived a new boundary condition for use in such cases based on considerations of local equilibrium, incorporating ideas introduced and used by Loper & Roberts (2001, though reported at meetings in 1996 and 1997 and available in preprint form in 1997) to identify the existence of a 'hidden mush', i.e. the fact that a steady-state chimney cannot extend all the way to the base of the mushy layer. Schulze & Worster (1999) further described in detail the complete set of interfacial boundary conditions required at steady mush–liquid interfaces depending on whether they are advancing or retreating and whether the flow is from mush to liquid or vice versa (see review by Worster 2002).

We use those boundary conditions here to calculate steady states in a two-

https://doi.org/10.1017/S0022112001007558 Published online by Cambridge University Press

dimensional mushy layer with chimneys, in which the upper mush–liquid interface and the chimney walls are completely free boundaries. These calculations are important in displaying the character of steady-state chimneys and in assessing the validity of various assumptions and approximations that have been made to model them more simply. We have performed our analysis in two dimensions for computational ease and for comparison with previous studies, though the methods we develop can readily be adapted to three dimensions.

In common with some earlier studies (Roberts & Loper 1983; Worster 1991; Fowler 1997; Schulze & Worster 1998), we use lubrication theory to analyse the chimney and emerging plume. We then use the results of those analyses to determine boundary conditions for the exterior liquid and mushy regions, which are analysed numerically. We can thus significantly reduce both the grid storage and the computation time, which are usually the greatest impediments to highly resolved numerical calculations. This has enabled us to make much more detailed calculations and to cover a wide range of parameter space with greater ease than would have been possible using a fully numerical approach.

The mathematical formulation is presented in § 2, together with an analysis of the chimney and plume, and the numerical method is described in § 3. We present the numerical results and discuss some findings and their relationships with previous work in § 4. In § 5 we formulate the equations governing the structure of internal liquid inclusions (incipient chimneys). Our results elucidate the nature of the flow, pressure and thermal fields in the neighbourhood of the mush–liquid interface, an understanding of which may allow future models to be developed in which detailed calculations of the entire liquid region are unnecessary (§ 6). Finally, a summary and conclusions are given in § 7.

2. Mathematical formulation

Consider a two-dimensional system, as shown in figure 1, in which a binary mixture of initial concentration C_0 is pulled downwards at a steady rate V between fixed heat exchangers. The lower heat exchanger is at a temperature less than the eutectic temperature T_E, which causes the mixture to be completely solid there. The upper heat exchanger maintains the temperature of the mixture far above the solidification front at a value T_0 greater than the liquidus (freezing) temperature $T_L(C_0)$, so that the mixture is entirely liquid there. In this configuration, a mushy layer is sandwiched between the liquid region above and the solid (eutectic) region below. We look for states that are horizontally periodic and steady in the frame of reference of the heat exchangers, and allow for chimneys to form at one of the vertical boundaries of the periodic cell. Note that, whereas the solid–mush and mush–liquid interfaces are stationary in this frame of reference, the solid layer and the solid matrix of the mushy layer have velocity $\boldsymbol{V} = -V\boldsymbol{k}$, where $\boldsymbol{k}$ is a unit vector in the vertical z-direction. This configuration is representative of continuous and directional casting, though it is adopted here principally because it is most suitable for studies of stability and bifurcation. An alternative configuration, in which solidification proceeds from a cooled boundary, is more representative of static castings and most laboratory experiments to date (e.g. Huppert 1990; Chen 1995; Bergman *et al.* 1997; Solomon & Hartley 1998). Since in those cases the system is always in a transient state, the present analysis will not apply in detail, though many important principles are transferable between the two configurations.

We treat the mushy layer as being *ideal* (Worster 1997) by assuming that the

https://doi.org/10.1017/S0022112001007558 Published online by Cambridge University Press

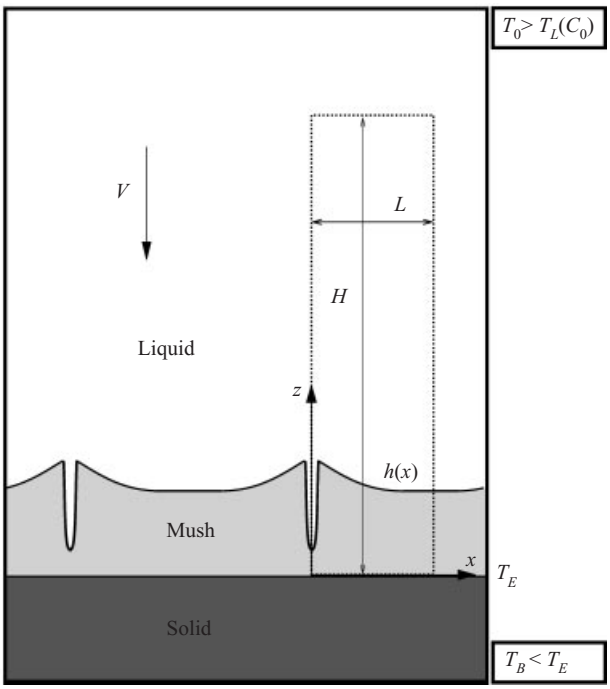


FIGURE 1. Schematic diagram of the system considered, showing the solid, mushy and liquid regions and the periodically distributed chimneys. The diagram is representative of directional solidification at constant speed V by pulling a mould through fixed heat exchangers.

temperature and concentration within it are tied to a linear liquidus, that the thermal properties and the density of solid and liquid are equal, that there is complete solute rejection upon solidification, and that it forms a locally isotropic porous medium in which the flow is governed by Darcy's equation. For simplicity, we make the further assumptions that solutal diffusion is negligible in both liquid and mushy regions, and that the Prandtl number is infinite, so that inertia is negligible in the liquid region. The former removes the boundary-layer mode of convection (Worster 1992), which complicates the motion of the liquid region and is not felt to influence chimneys directly. The latter assumption is not appropriate for metallic nor aqueous systems but is made here to simplify the numerics, following Schulze & Worster (1999). Finally, we ignore the thermal contribution to the buoyancy of the fluid, which can lead to complicating oscillatory and double-diffusive effects, to concentrate on the role of compositional buoyancy alone.

Dimensionless temperature and concentration variables are defined by

$$\theta = [T - T_L(C_0)]/\Delta T, \quad \Theta = (C - C_0)/\Delta C, \tag{2.1a,b}$$

where $\Delta C = C_0 - C_E$ is the difference between the far-field concentration and the eutectic concentration, and $\Delta T = T_L(C_0) - T_E = \Gamma \Delta C$ is the difference between the far-field liquidus temperature and the eutectic temperature, where Γ is the slope of the liquidus. Note that $\theta = \Theta$ in the mushy layer.

With the assumptions and approximations given above, the dimensionless equations governing conservation of heat, solute and momentum are

$$\nabla^2\theta + \theta_z = \boldsymbol{u} \cdot \nabla\theta + S\,\phi_z, \tag{2.2a}$$

https://doi.org/10.1017/S0022112001007558 Published online by Cambridge University Press

$$[(1-\phi)\theta + \mathscr{C}\phi]_z = \boldsymbol{u}\cdot\nabla\theta, \tag{2.2b}$$

$$\boldsymbol{u} = -R_m\Pi(\nabla p + \theta\boldsymbol{k}), \tag{2.2c}$$

in the mushy layer (Worster 1997), and

$$\nabla^2\theta + \theta_z = \boldsymbol{u}\cdot\nabla\theta, \tag{2.3a}$$

$$\Theta_z = \boldsymbol{u}\cdot\nabla\Theta, \tag{2.3b}$$

$$\nabla^2\boldsymbol{u} = \frac{R_m}{Da}(\nabla p + \Theta\boldsymbol{k}), \tag{2.3c}$$

in the liquid region, where ϕ is the solid fraction, $\boldsymbol{u}$ is defined as the fluid velocity relative to the solid matrix in the liquid region and as the Darcy velocity (volume flux) in the mushy region, and p is the pressure. These equations describe steady states in a frame of reference moving with the solidification speed. For numerical computations, we have chosen to use a vorticity–stream-function formulation and written equations (2.2c) and (2.3c) as

$$\nabla^2\psi = -R_m\Pi\theta_x + (\nabla\Pi\cdot\nabla\psi)/\Pi, \tag{2.4}$$

$$\nabla^2\omega = -\frac{R_m}{Da}\Theta_x, \quad \text{where} \quad \nabla^2\psi = -\omega, \tag{2.5a,b}$$

ω is the vorticity component normal to the two-dimensional plane, and ψ is the two-dimensional stream function defined by $\boldsymbol{u} = (-\psi_z, \psi_x)$.

These equations have been made dimensionless by scaling velocities with V, distances with κ/V (where κ is the thermal diffusivity), pressure with $\beta\Delta C\rho_0 g\kappa/V$ (where β is the solutal expansion coefficient, ρ_0 is a representative density and g is the acceleration due to gravity), and permeability

$$\Pi = (1-\phi)^3 \tag{2.6}$$

with a reference value Π_0. This form of the permeability function is approximate but has been used before for analytical convenience (e.g. Fowler 1985; Worster 1992). The dimensionless parameters in these equations are

$$S = \frac{\mathscr{L}}{c_p\Delta T}, \quad \mathscr{C} = \frac{C_s - C_0}{\Delta C}, \quad R_m = \frac{\beta\Delta C g\Pi_0}{\nu V}, \quad Da = \frac{\Pi_0 V^2}{\kappa^2}, \tag{2.7a–d}$$

where $\mathscr{L}$ is the latent heat of solidification, c_p is the specific heat capacity, C_s the constant solute concentration in the solid phase of the mushy layer, and ν is the kinematic viscosity of the liquid.

We seek solutions for a half-cell of the periodically extended system. This is shown schematically in figure 2, in which the chimney and plume have been collapsed to the line $x = 0$ as described below. The symmetry line on the vertical boundary dividing two adjacent convective cells is denoted by $x = L$, where the boundary conditions are the symmetry conditions

$$\psi = \theta_x = 0 \quad \text{at} \quad x = L, \quad z < h(L), \tag{2.8a}$$

$$\omega = \psi = \theta_x = 0 \quad \text{at} \quad x = L, \quad z > h(L), \tag{2.8b}$$

in which $h(x)$, the height of the mushy layer, is an unknown function that must be calculated. These conditions represent the fact that there is no flow ($\psi = 0$) and no heat flux ($\theta_x = 0$) across the periodic boundary, and that there is no stress ($\omega = 0$) in the liquid region there.

https://doi.org/10.1017/S0022112001007558 Published online by Cambridge University Press

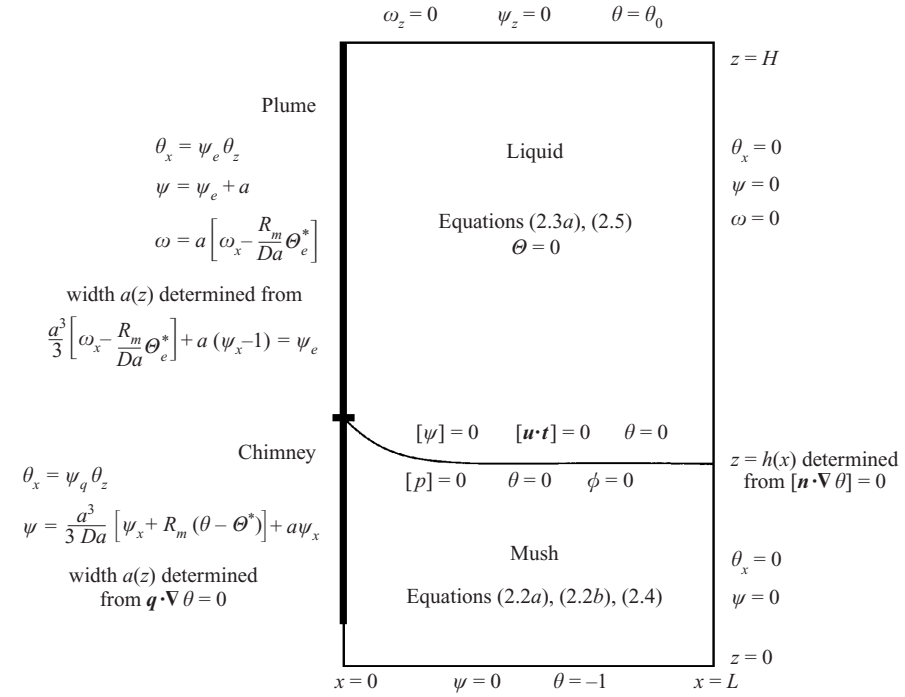


FIGURE 2. The computational domains used for the numerical calculations in the mush and liquid regions, showing the boundary conditions applied. The boundary conditions at $x = 0$ are derived from lubrication analyses of the chimney and plume.

At the solid–mush interface, the normal component of the Darcy velocity is zero, and the temperature and concentration are fixed at their eutectic values. Thus, we have

$$\psi = 0, \quad \theta = -1 \quad \text{at} \quad z = 0. \tag{2.9}$$

In the far field (numerically denoted by $z = H \gg 1$), we assume the pressure to be independent of the horizontal direction and the flow to be purely vertical. The temperature and concentration take their far-field values there. Thus

$$\omega_z = \psi_z = \Theta = 0, \quad \theta = \theta_0 \quad \text{at} \quad z = H. \tag{2.10}$$

Since we are ignoring solutal diffusivity, solute is conserved along streamlines of $\boldsymbol{q} = \boldsymbol{u} + \boldsymbol{V}$ in the liquid region. This can be seen from (2.3b), which can be written in the form $\boldsymbol{q}\cdot\nabla\Theta = 0$. The vector field $\boldsymbol{q}$ is the total material volume flux; it is the fluid velocity in the liquid region but is the mean volume flux of material (regardless of phase) in the mushy region. All such streamlines impinging on the mush–liquid interface (not including the chimney wall) originate in the far field, which implies that the liquid concentration at the interface is equal to its far-field value $\Theta = 0$. Conservation of heat and solute, coupled with the principle of marginal equilibrium – that the mushy layer grows sufficiently rapidly to eliminate any constitutional supercooling in the liquid – yield the additional boundary conditions†

$$\phi = \theta = [\boldsymbol{n}\cdot\nabla\theta]_m^l = 0 \quad \text{at} \quad z = h(x), \tag{2.11a–c}$$

† The fact that the condition $\phi = 0$ follows from the weak constraint $\partial T/\partial n \geqslant \partial T_L/\partial n$ in most circumstances, including the important limit $D/\kappa \to 0$, is discussed by Worster (2000) and in more detail by Loper (2001).

https://doi.org/10.1017/S0022112001007558 Published online by Cambridge University Press

while the hydrodynamic boundary conditions are given by

$$[\psi]^l_m = [p]^l_m = [\boldsymbol{u}\cdot\boldsymbol{t}]^l_m = 0 \quad \text{at} \quad z = h(x), \tag{2.12a–c}$$

where $\boldsymbol{n}$ is the unit normal and $\boldsymbol{t}$ is a unit tangent vector to the mush–liquid interface, see Schulze & Worster (1999), Worster (2002).

When the flow is weak, before a chimney forms, the boundary conditions at $x = 0$ are equivalent to the symmetry conditions (2.8). At larger amplitudes, when the vertical component of the dynamic velocity $\boldsymbol{u}$ has exceeded the solidification rate sufficiently, an internal region of the mushy layer is dissolved into a liquid inclusion, and ultimately a chimney forms (Schulze & Worster 1999). Once there is a chimney with a plume emanating from it, the boundary conditions at $x = 0$ are modified as follows.

The chimney

A significant feature of chimneys observed in experiments is that they are narrow compared with their length, so lubrication theory can be used to analyse the flow within them. With an assumption of small Péclet number in the chimney (expressed dimensionlessly as $\psi_q \ll 1$, where $\psi_q = \psi - x$ is the stream function associated with $\boldsymbol{q}$), the temperature is approximately uniform across it. The balance of vertical advection of heat with its conduction through the chimney walls then gives

$$\theta_x = \psi_q \theta_z \quad \text{at} \quad x = a. \tag{2.13}$$

It is interesting to note that this relationship implies that the slope of an isotherm (for example the upper mush–liquid interface) at the chimney wall is equal to the negative of the stream function there: $\partial z/\partial x|_\theta = -\psi_q$.

The value of the stream function at the chimney wall is determined by integrating equation (2.3*c*), which can be written in the lubrication approximation as

$$\psi_{xxx} = \frac{R_m}{Da}(p_z + \Theta), \tag{2.14}$$

where p_z is constant across the chimney. We assume a top-hat profile $\Theta = \Theta^*(z)$ and integrate (2.14), subject to the conditions $\psi = \psi_{xx} = 0$ at $x = 0$, continuity of vertical velocity at the chimney wall, and using Darcy's equation (2.2*c*) to eliminate the pressure term, to give

$$\psi = \frac{a^3}{3Da}\left[\frac{\psi_x}{\Pi} + R_m(\theta - \Theta^*)\right] + a\psi_x \quad \text{at} \quad x = a. \tag{2.15}$$

This expression reflects the well-known properties of two-dimensional lubrication flows that the volume flux is proportional to the pressure gradient and to the cube of the width of the channel (Batchelor 1967). Note that the term $a\psi_x$ on the right-hand side, included to match the vertical velocity on the mush side of the chimney wall, is $O(Da/a^2)$ relative to the first term in square brackets and is therefore formally negligible according to the continuum hypothesis on which the model of the mushy region is developed. Neglecting it is equivalent to applying the no-slip condition at the chimney wall to the flow inside the chimney. However, we include it here, for use in (2.16) and (2.17) below, since it dominates the expression near $a = 0$ and is required to avoid ψ_q becoming unphysically negative near the base of the chimney.

Expression (2.15), without the final term, is the same as equation (17.94) of Fowler (1997) when thermal buoyancy is neglected, as here, and once it is recognized that $\phi = 0$ on the chimney wall, so that $\Pi = 1$. Expressions with slightly different

https://doi.org/10.1017/S0022112001007558 Published online by Cambridge University Press

coefficients were derived by Roberts & Loper (1983), Worster (1991) and Schulze & Worster (1998) from different shape assumptions for the compositional profile, though, importantly, the functional relationship is the same in all cases. Loper & Roberts (2001) consider a limit in which the resistance to flow through the mushy layer is negligible compared with the resistance within the chimney. In this case, the pressure-gradient term in (2.14) can be neglected and they were able to determine an exact solution to the resulting equation.

The value of the mean composition Θ^* in the chimney is determined from conservation of solute,

$$\psi_q \Theta^* = \int_0^{\psi_q} \Theta \, \mathrm{d}\psi_q, \tag{2.16}$$

noting that (2.3b) implies that solute is conserved along streamlines of $\boldsymbol{q}$, i.e. that $\Theta = \Theta(\psi_q)$.

Note that (2.13) and (2.15) reduce to the symmetry conditions $\theta_x = \psi = 0$ when $a = 0$, i.e. where there is no chimney.

The boundary conditions (2.13) and (2.15), which are expressions of heat and mass conservation for the chimney, can be applied once the width of the chimney $a(z)$ is known. Roberts & Loper (1983) prescribed a constant value for a and examined the consequent flow. Schulze & Worster (1998) assumed that a was independent of z but adjusted its value until the solid fraction ϕ was zero at a single point on the chimney wall, arbitrarily chosen to be at mid-height.

Loper & Roberts (2001) showed that when, as here, solutal diffusion is neglected, $(\boldsymbol{n} \cdot \boldsymbol{k})\phi = 0$ on the chimney wall, where $\boldsymbol{k}$ is a unit vector in the vertical direction. They interpreted this as showing that the chimney wall is vertical to leading order, leaving the solid fraction non-zero. They subsequently determined the width of the chimney to eliminate a singularity at its vent that arises from the retention of a term proportional to the diffusion of solute.

Conversely, Schulze & Worster (1999) argued from conservation of solute in the limit of negligible solute diffusion that $\phi = 0$ at any solidifying mush–liquid interface where the flow, $\boldsymbol{q}$, is from mush to liquid, as typified by the steady-state chimney wall.

In addition to their main analysis, Loper & Roberts (2001) give physical reasons for the existence of a 'hidden mush' between the bottom of a steady-state chimney and the eutectic front. Schulze & Worster (1999) extended those ideas, which had been made public by Loper & Roberts at lectures and seminars in 1996 and 1997, to show that $\boldsymbol{q} \cdot \nabla\theta \geqslant 0$ at the chimney wall. Schulze & Worster (1999) showed further that the solid fraction on the mush side of the chimney wall would be negative unless $\boldsymbol{q} \cdot \nabla\theta \leqslant 0$. These two conditions – that the liquid in the chimney be not supercooled and that the solid fraction in the mushy layer be non-negative – combine to show that streamlines of $\boldsymbol{q}$ must enter the chimney parallel to isotherms, i.e. that

$$\boldsymbol{q} \cdot \nabla\theta = 0 \quad \text{at} \quad x = a. \tag{2.17}$$

This is the case when the chimney wall is a solidifying interface ($a_z > 0$) and the flow, $\boldsymbol{q}$, is directed from the mush into the chimney. We use (2.17) to determine the local value of $a(z)$, noting from (2.2b) that it automatically implies that $\phi \equiv 0$ on the chimney wall.

The plume

We adopt a similar lubrication analysis for the plume emanating from the chimney. Since solutal diffusion is ignored, the edge of the plume is readily identified with the

https://doi.org/10.1017/S0022112001007558 Published online by Cambridge University Press

streamline of $\boldsymbol{q}$ that passes through the corner of the chimney opening, which is also the solute contour $\Theta = 0$. Thus the volume flux in the plume ψ_q is independent of height and equal to the volume flux exiting the chimney $\psi_e \equiv \psi_q(a, h(a))$. Similarly, the mean (top-hat) concentration $\Theta^* = \Theta_e^*$, defined in (2.16), is independent of height in the plume and equal to its value at the chimney vent. We integrate (2.14) across the plume, subject to the boundary conditions $\psi = \psi_{xx} = 0$ at $x = 0$ and continuity of vertical velocity at the edge of the plume, and use (2.3*c*) to eliminate the pressure term, to give

$$\omega = a\left(\omega_x - \frac{R_m}{Da}\,\Theta_e^*\right) \quad \text{at} \quad x = a, \tag{2.18}$$

with

$$\psi = \psi_e + a = \frac{a^3}{3}\left(\omega_x - \frac{R_m}{Da}\,\Theta_e^*\right) + a\,\psi_x \quad \text{at} \quad x = a. \tag{2.19}$$

Equation (2.19) is used to determine the width of the plume $a(z)$ for use in the vorticity boundary condition (2.18). Equation (2.13) applies similarly at the edge of the plume to give

$$\theta_x = \psi_e \theta_z \quad \text{at} \quad x = a. \tag{2.20}$$

These interface conditions at the edge of the chimney and plume complete the mathematical description of the problem. We proceed to solve equations (2.2)–(2.5) numerically, using the fact that $a \ll 1$ to apply the interface conditions at $x = 0$. By this means, the chimney and plume are treated as singular interfaces, each with a single internal parameter, its width $a(z)$.

3. Computational procedures

The equations and boundary conditions to be solved numerically are summarized in figure 2. We employed coordinate transformations to convert the free-boundary problem for the mush–liquid interface into fixed domains. Each of the mushy and liquid regions was transformed to a unit square using

$$\xi = \frac{x}{L}, \quad \zeta = \frac{z}{h(x)} \tag{3.1a, b}$$

for the mushy region and

$$\xi = \frac{x}{L}, \quad \zeta = \frac{H - z}{H - h(x)} \tag{3.2a, b}$$

for the liquid region. The governing equations were discretized by second-order, finite-difference formulae on a fixed grid in each domain and solved by iteration.

Equations (2.2*a*) and (2.4) for the thermal and velocity fields in the mushy region were solved by the Gauss–Seidel method with successive over-relaxation (Press *et al.* 1988). The nonlinear terms, including those introduced by the coordinate transformation (3.1), were evaluated at each iteration using data from the previous iteration. The solid fraction ϕ was determined by integrating equation (2.2*b*) downwards from the mush–liquid interface $z = h(x)$ ($\zeta = 1$). A strong flow occurs in the liquid region once the plume forms, which can cause the Gauss–Seidel method to lose its diagonal dominance and cause the computation to diverge. We therefore used an ADI (alternating direction implicit) scheme (Press *et al.* 1988) instead to solve equations (2.3*a*) and (2.5*a*, *b*).

Each iteration described above was performed for fixed $h(x)$ and $a(z)$ in each

https://doi.org/10.1017/S0022112001007558 Published online by Cambridge University Press

domain. Between iterations, these free-boundary parameters were updated using the pseudo-time derivatives

$$\frac{\partial h}{\partial t} = \epsilon_1 \left[\boldsymbol{n} \cdot \nabla\theta\big|_{h-} - \boldsymbol{n} \cdot \nabla\theta\big|_{h+} \right], \tag{3.3a}$$

$$\frac{\partial a}{\partial t} = \epsilon_2 \boldsymbol{q} \cdot \nabla\theta\big|_{x=0} \quad \text{in } z < h(0), \tag{3.3b}$$

$$\frac{\partial a}{\partial t} = \epsilon_3 \left[\psi_e - \frac{a^3}{3} \left(\omega_x - \frac{R_m}{Da} \Theta_e^* \right) - a(\psi_x - 1) \right]_{x=0} \quad \text{in} \quad z > h(0), \tag{3.3c}$$

where t is an iteration time and the relaxation parameters ϵ_i ($i = 1, 2, 3$) were adjusted to ensure convergence of the numerical scheme to a steady state. If a negative value of a would be predicted from (3.3b) then the value of a was set to zero. It is clear that once a steady state is reached, the interfacial conditions (2.11c), (2.17) and (2.19), which form the right-hand sides of equations (3.3), are satisfied. Although the widths of the chimney and plume are scaled to zero in the computational domain, the functional parameters describing them still influence the system's evolution through the corresponding boundary conditions. In order to achieve convergence, we found that it was necessary to limit the size of the ϵ_i. Though no formal bounds were derived, we could achieve convergence using $\epsilon_1 = 0.4$, $\epsilon_2 = 0.02$, and $\epsilon_3 = 1$, with the dimensionless time step of the iteration taken to have the same value as the grid spacing.

We wished to trace out as much of the finite-amplitude bifurcation diagram as we could. In order to converge to the unstable portions of the bifurcation curve, we followed Schulze & Worster (1999) and employed a continuation scheme. That is, instead of specifying the Rayleigh number, we solved for it having fixed the value of the stream function at a specified grid point. Schulze & Worster (1999) suggested that the best convergence is achieved when the chosen point is a little below the centre of the mushy region. We also found that this choice is best before the chimney forms. However, once the chimney occurs, it is much better to choose the grid point close to the upper left corner of the computational domain (near the chimney vent). The reason is that after the occurrence of a chimney, the maximum value of the stream function in the mushy region moves towards the chimney vent. In consequence, the stream function in the central region no longer increases monotonically along the solution curve, which makes the continuation scheme harder to follow. The scheme was initialized by fixing ψ and ω equal to zero to obtain the pure conductive solution. Other variables were calculated by iteration, all starting at zero except for h, which was initially set to have a finite value, say 1.5. To avoid (3.3a) breaking down at the initial stage of the iteration because the temperature derivatives are initially zero at the interface, we by-passed this equation until the temperature derivatives became finite-valued. After obtaining the pure conductive solution, the continuation scheme was applied to obtain the convective solutions.

All the computations were performed on a uniform mesh that had 41 grid points in both the vertical and horizontal directions unless otherwise stated. Mesh refinement was used to check the accuracy for selected computations. For example, for $R_m = 12.9$, the salt flux through the chimney computated by the mesh of 41×41 deviated from that computed with a mesh of 74×74 by only 0.4%. For most of our calculations, the height of the domain was fixed at $H = 5$. We also increased H to assess its influence for selected computations. For example, for $R_m = 13$, we found that the salt

https://doi.org/10.1017/S0022112001007558 Published online by Cambridge University Press

flux calculated by setting $H = 5$ was only about 5% lower than that computed with $H = 10$. Using a mesh of 41×41 grid points, it took approximately 5 minutes on a DEC Alpha workstation to converge to each stable steady state and approximately 20 minutes to converge to each unstable steady state using the continuation scheme.

4. Discussion of computational results

For all the results given in this paper, we have used the parameter values $\mathscr{C} = 15$, $S = 5$, $\theta_0 = 0.4$ and $Da = 0.005$. All but the Darcy number are representative of laboratory experiments using aqueous solutions of ammonium chloride. The Darcy number in such experiments is of order 10^{-5}. In our calculations, the Darcy number principally affects the flow of the plume in the liquid region, which is characterized by a fluid Rayleigh number R_m/Da. The value we used was a compromise between requiring a small value for Da while not expending too much of the computational effort resolving the liquid region, which has little influence on the mushy layer and chimney. For the main results, we used a value of $L = 2.16$ corresponding to the critical wavelength for linear stability, given the parameter values above. Apart from the Darcy number, these parameter values are the same as those used by Schulze & Worster (1999).

Some typical results are shown in figure 3, for a Rayleigh number of 12.92. At this Rayleigh number there are two steady states, shown in figures 3(a, b) and 3(c, d) respectively. On the left of figures 3(a) and 3(c), we show streamlines of $\boldsymbol{u}$ (solid lines) and solid-fraction contours (dashed lines). On the right of these figures, we show streamlines of $\boldsymbol{q}$ (solid lines) and isotherms (dashed lines). Figures 3(b) and 3(d) show the widths of the chimney (solid lines) and plume (dashed lines).

The first set of figures (3a, b) corresponds to a convecting state with no chimney, and is directly comparable to figure 3 of Schulze & Worster (1999). It occurs on a lower branch of a subcritical bifurcation curve (see figure 5 below), so is likely to be unstable. The streamlines of $\boldsymbol{u}$ have the characteristic shape of convective normal modes, corresponding to the mushy-layer mode of convection (Worster 1992). The streamlines of $\boldsymbol{q}$ are all flowing downwards, showing that all material elements are ultimately solidified in this state. Notice that the mush–liquid interface has the 'hummocky' appearance seen experimentally by Tait, Jahrling & Jaupart (1992) prior to the formation of chimneys, and that the solid fraction is small in a region around $x = 0$, signalling the incipient appearance of a chimney.

The second set of figures (3c, d) corresponds to a state with a fully developed chimney. Note that the chimney does not extend to the bottom of the mushy layer, in agreement with the prediction (Loper & Roberts 2001) of a region of 'hidden mush' below the chimney. Some of the $\boldsymbol{q}$-streamlines that originate from the liquid region enter the chimney and ultimately exit the domain via the plume. Material elements along such streamlines are partially solidified during their traverse of the mushy region and ultimately rejoin the liquid region depleted of solute. Therefore, in contrast with the first state, which causes only lateral macrosegregation, this state causes vertical redistribution of solute. In this state, the mush–liquid interface forms a volcano-shaped vent around the plume at the top of the chimney, which is a characteristic feature seen in laboratory experiments (Copley *et al.* 1970; Huppert 1990; Chen & Chen 1991). Finally, note that the solid fraction increases a little as the chimney is approached horizontally before ultimately decreasing to zero in a very narrow region near the chimney wall. The increase in solid fraction, which is due to cooling from the liquid rising in the chimney, has been observed in experiments (Chen 1995), and was

https://doi.org/10.1017/S0022112001007558 Published online by Cambridge University Press

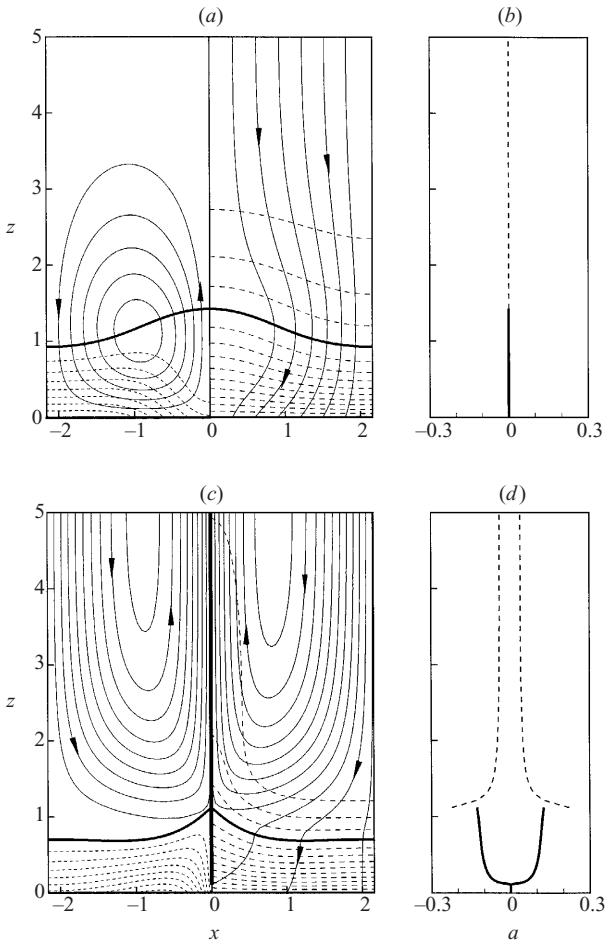


FIGURE 3. The flow, temperature and solid-fraction fields for $R_m = 12.917$, $\mathscr{C} = 15$, $S = 5$, $\theta_0 = 0.4$, $Da = 0.005$, and $L = 2.16$. There are two steady states at this Rayleigh number; see text for details. On the left of (a) and (c) are streamlines of $\boldsymbol{u}$ (solid curves) and contours of solid fraction (dashed curves). On the right are streamlines of $\boldsymbol{q}$ (solid curves) and contours of temperature (dashed curves). The mush–liquid interface is shown with a heavy solid curve. Plotted in (b) and (d) are the widths of the chimney (solid curves) and the plume (dashed curves) as functions of z. The values of the isotherms are from $\theta = -1$ to 0.3 by 0.1 increments, starting from the bottom. The contour values of solid fraction begin at 0 from the top of the mushy layer, then increase downwards by 0.01 increments. The contour increment for the streamlines on the right-hand side of (a) is 0.3, while on the left-hand side is 0.1. The contour increment for the streamlines in (c) is 1.

predicted by the scaling analysis of Worster (1991) and the numerical calculations of Schulze & Worster (1998). Many of the qualitative features of figure 3(c), including the shapes of the isotherms, are comparable to the experimental observations made by Solomon & Hartley (1998).

The width of the plume is not continuous with the width of the chimney (figure 3d) since it is more appropriate in the lubrication analyses used to model these to match their mass and solute fluxes. A local analysis that does not employ the lubrication approximation would be necessary to connect these exit and entry conditions more precisely. There is some acceleration and narrowing of the plume as it rises, though, within a distance of only a few widths, its width reaches a uniform value equal to

https://doi.org/10.1017/S0022112001007558 Published online by Cambridge University Press

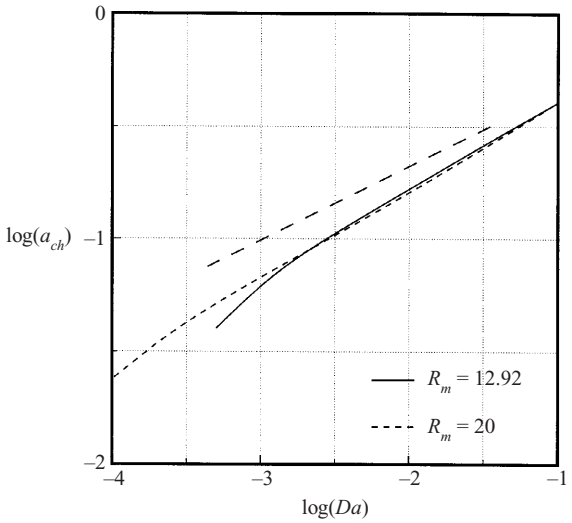


FIGURE 4. The width of the chimney (at its vent) as a function of Darcy number for two different values of the Rayleigh number. The long-dashed line has a slope of 1/3.

about a third of the width of the chimney. Note the exaggerated horizontal scale of figure 3(*d*); the width of the plume is only about 0.1, comparable in magnitude to $Da^{1/3}$. In figure 4, we show the width of the chimney as a function of the Darcy number for two fixed Rayleigh numbers. We see that the width scales approximately as $Da^{1/3}$, which is the asymptotic result obtained by Schulze & Worster (1998) in the limit of large Rayleigh number.

It is evident from figure 3(*c*) that flow in the liquid region is driven much more strongly by viscous coupling with the plume, once it forms, than by the need to replace the buoyantly convecting fluid from the mushy layer. This is likely to be a result of the fact that we have assumed a Stokes flow in the liquid region. Much weaker coupling with the motion of the plume is likely in fluids with lower Prandtl numbers.

In figure 5(*a–e*), we plot various properties of the system as the Rayleigh number is varied. The topology and many other properties of the flow change significantly once there are chimneys, making it difficult to find a single measure of the amplitude of convection that is meaningful in both circumstances.

We begin, in figure 5(*a*), by showing the maximum value of the stream function $\psi_{\max}$ in the combined domain (liquid plus mush). There is a subcritical bifurcation from the linear critical point at $R_m = 13.04$, shown enlarged in the inset. Just after point A (where $R_m = 12.92$, corresponding to figure 3*a*, *b*) a region of negative solid fraction occurs around $x = 0$, about halfway up the mushy layer (Schulze & Worster 1999). Such unphysical solutions of the mathematical model can be continued as shown by the dashed portion of the curve. As described above (figure 3*c*, *d*), there is a second solution with $R_m = 12.92$, indicated by point B in figure 5(*a*). This solution, which has a fully developed chimney, has a much larger value of $\psi_{\max}$, which occurs in the liquid region rather than in the mushy layer, and results from the strong forcing of the plume. We followed the solution curve from B in both directions as shown. Tracing backwards along it, the curve passes through a turning point at $R_m = 11.1$, labelled R_g, which represents the smallest value of the Rayleigh number (for the given

https://doi.org/10.1017/S0022112001007558 Published online by Cambridge University Press

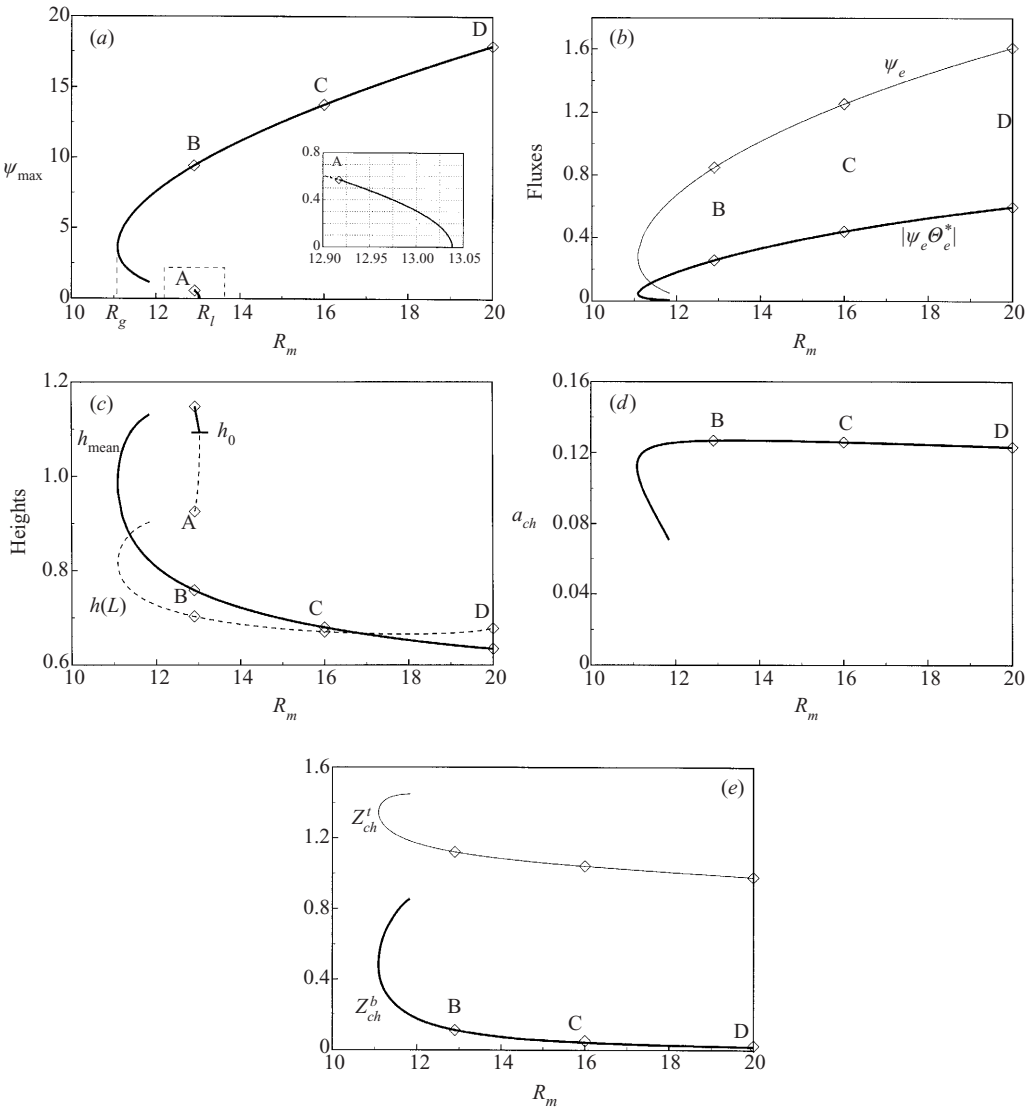


FIGURE 5. A plot of (*a*) $\psi_{\max}$ the maximum value of stream function, (*b*) $|\psi_e \Theta_e^*|$ the solute flux (thick curve) and ψ_e the volume flux (thin curve) through a chimney, (*c*) the mean height of the mushy layer (solid curve) and $h(L)$ the mushy layer height at $x = L$ (dashed curve), (*d*) a_{ch} the maximum chimney width, (*e*) Z_{ch}^b the bottom position (thick curve) and Z_{ch}^t the top position (thin curve) of a chimney, as functions of the Rayleigh number. The other parameters are the same as used for figure 3. The curve enclosed by dashed lines is enlarged in the inset in (*a*). The detailed flow information of the points labelled A and B is shown in figures 3(*a*, *b*) and 3(*c*, *d*) respectively and that of the points labelled B, C and D is shown in figure 6(*a*–*c*).

parameters) at which finite-amplitude, steady states of the form described here can exist.

We were unable to continue the lower branch of chimney solutions backwards beyond $R_m = 11.84$, $\psi_{\max} = 1.2$. This may be a consequence of the continuation scheme we were using or may be an indication that no steady states exist connecting this point to the branch of convecting solutions without chimneys. When we tried

https://doi.org/10.1017/S0022112001007558 Published online by Cambridge University Press

to compute solutions in this region, we found that the numerical scheme oscillated between states with and without a chimney and finally failed to converge.

Once the chimney has formed, two important measures of the amplitude of convection are the mass and solute fluxes emanating from the chimney. These are displayed as ψ_e and $|\psi_e \Theta_e^*|$ in figure 5(b). Recall that the assumption of small Péclet number used to derive (2.13) and (2.20) requires that $\psi_e \ll 1$, so we see that this approximation becomes poorer at larger Rayleigh numbers. This needs to be addressed if better quantitative results are required. The solute exiting the chimney entered it at different heights along the chimney wall, making Θ_e^* a weighted average (defined by (2.16)) of the concentrations of the different fluid parcels. It is evident from figure 5(b) that Θ_e^* is rather less than 0.5, indicating, perhaps not surprisingly, that more of the fluid entered the chimney in the upper half of the mushy layer.

In figure 5(c) we show with a solid curve the mean dimensionless height of the mushy layer. Before the chimney forms, the interface is raised where there is upflow, near $x = 0$, and depressed where there is downflow, near $x = L$. Overall, the mean dimensionless height of the mushy layer increases with the strength of convection, probably because the upflow, coming through a region of lower solid fraction, is more potent in affecting the thermal transfer from the liquid region. However, once the chimney forms, the mean dimensionless height decreases monotonically with the strength of convection. Note, however, that the physical (dimensional) height of the mushy layer, proportional to R_m as the solidification rate varies for fixed physical parameters, increases monotonically with the strength of convection. Shown with a dashed curve is the dimensionless height of the mushy layer at the symmetry line $x = L$. Although this also decreases initially as the strength of convection increases along the chimney branch, we see that it begins to increase again after $R_m = 18$. This increase is associated with a secondary convection cell, described in figure 6(c) and the associated text below.

The curve in figure 5(d) shows the maximum dimensionless width of the chimney (at its vent). This increases with the strength of convection on the lower branch, as also found by Schulze & Worster (1998). However, we were able to compute to significantly larger Rayleigh numbers and found that the dimensionless chimney width ultimately decreases with R_m along the upper branch. This latter trend is consistent with previous scaling analyses (Worster 1991; Schulze & Worster 1998) and with the results of laboratory experiments using a lead–tin alloy (Bergman *et al.* 1997). The initial increase in a is caused by enhanced dissolution of the crystals as the strength of upflow increases around the chimney. The latter narrowing occurs as the flow entrained into the chimney compresses the cold thermal boundary layer around it.

The positions of the bottom Z_{ch}^b and top Z_{ch}^t of the chimney are plotted in figure 5(e). Both decrease with the strength of the convection. The position of the vent decreases along with the overall height of the mushy layer (see figure 5c), and for similar reasons. The position of the bottom is located at a stagnation point of $\boldsymbol{q}$ on the axis $x = 0$, where $\boldsymbol{q} \cdot \boldsymbol{k} = \boldsymbol{u} \cdot \boldsymbol{k} - 1 = 0$. Since $\boldsymbol{u} \cdot \boldsymbol{k} = 0$ on $z = 0$ and increases upwards, it is clear that the stagnation point moves down as $|\boldsymbol{u}|$ increases. Note that, though the bottom of the chimney is always above the base of the mushy layer, they become very close as R_m increases. In experiments, chimneys have generally been seen extending all the way to the bottom. This may be a consequence of them extending too close to the bottom for the difference to be observed or because these experiments were transient with consequently different thermal and velocity fields.

Figure 6 shows the development of the mushy layer as the Rayleigh number increases. The flow in the liquid region becomes ever stronger but remains qualitatively

https://doi.org/10.1017/S0022112001007558 Published online by Cambridge University Press

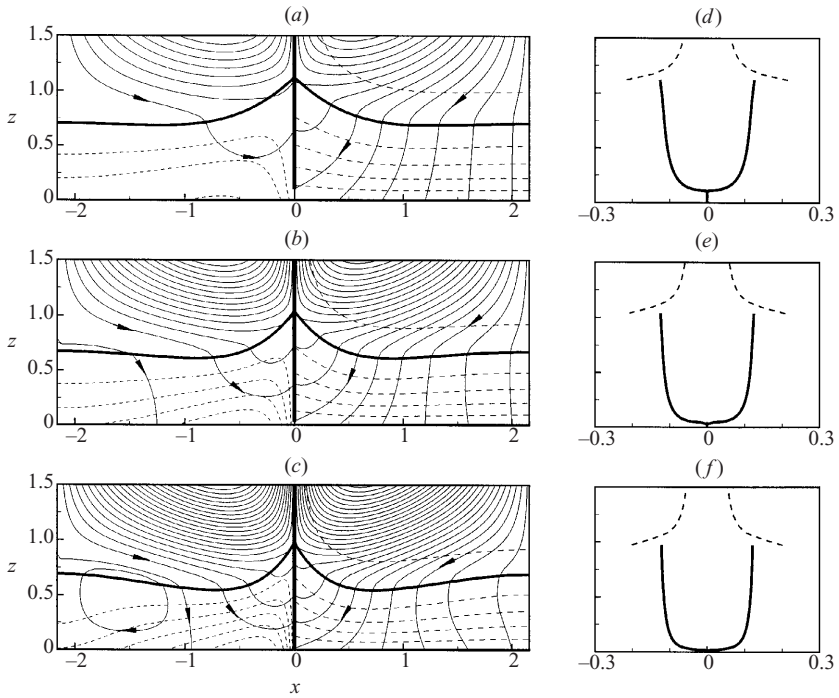


FIGURE 6. The flow, temperature and solid-fraction fields in the mushy layer for (*a*) $R_m = 12.9$, (*b*) $R_m = 16$ and (*c*) $R_m = 20$, corresponding to points B, C and D on figure 5. The remaining parameter values and the definitions for the different sorts of contours are the same as those in figure 3. We have used a 74×74 mesh to make the streamlines near the top of the mushy layer smooth. The values of the isotherms are from $\theta = -1$ to 0.2 by 0.2 increments, starting from the bottom. The contour values of solid fraction begin at 0 from the top of the mushy layer and increase downwards by 0.02. The contour increment for all the streamlines is 0.4 except for the two at the left lower corner of (*c*), where it is 0.1. In (*d*), (*e*) and (*f*) are shown the chimney profiles. The walls are almost vertical through most of the layer but the base of the chimney closes off just above the eutectic front.

unchanged from that shown in figure 3(*c*), so we have excluded most of that region from these figures.

Notice that the solid fraction increases from a maximum of about 0.06 at $R_m = 12.92$ to just under 0.12 at $R_m = 20$. Such an increase once convection through chimneys occurs was measured by Wettlaufer, Worster & Huppert (1997). It is significant too that Chen (1995) measured solid fractions of about 0.4 in an ammonium-choride mushy layer well after chimneys had been established, whereas the solid fraction prior to convection is predicted to have been only about 0.05. The solid-fraction contours also become more concentrated around the chimney as the Rayleigh number increases.

There has been some discussion on whether the flow in the mushy region is driven principally by the buoyancy in the chimney with the chimney acting as a sink to the outer flow (e.g. Worster 1991; Loper & Roberts 2001), or whether the chimney acts as a passive conduit for the convective flow in the mushy region driven by its own internal buoyancy (e.g. Schulze & Worster 1997). Another way of expressing this is whether the pressure gradient or the buoyancy dominates the right-hand side of (2.2*c*). In the former case, the flow towards the chimney would decay exponentially away from the chimney with a characteristic length comparable to the height of the layer, whereas in the latter case the variation of horizontal velocity would be algebraic between

https://doi.org/10.1017/S0022112001007558 Published online by Cambridge University Press

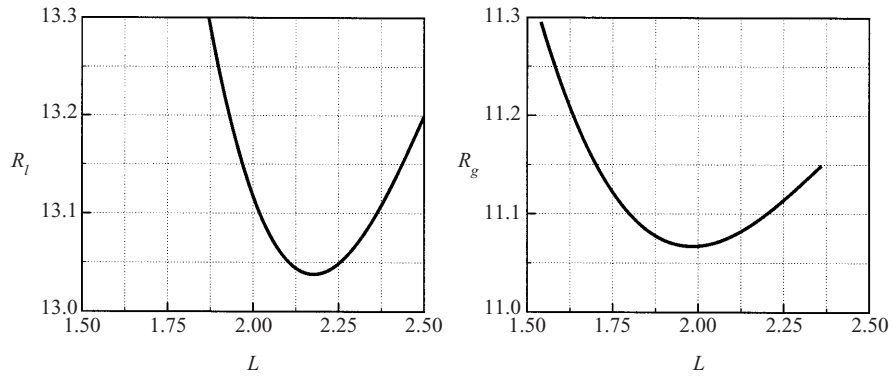


FIGURE 7. The linear R_l and global R_g critical Rayleigh numbers as function of the wavelength L. The parameter values are the same as those used in figure 3.

the chimney and the symmetry line, being part of a buoyancy-driven convection cell. Our results indicate that the chimney is passive at small convective amplitudes but becomes the driving agent of convection at larger amplitudes. It is clear from figure 6 that, at least at the higher Rayleigh numbers, the Darcy flow $\boldsymbol{u}$ is localized to a region of approximately unit aspect ratio around the chimney. The interstitial fluid further from the chimney is almost stagnant and even displays a weak counter-rotating convection cell in figures 6(b) and 6(c). In figure 6(c) it is evident that the reverse flow is causing a diminution of the solid fraction near the symmetry line, and the mush–liquid interface is raised a little (see also figure 5c). We can anticipate that at even higher Rayleigh numbers a new chimney will form there.

It is clear that when convection is weak, certainly before the chimney forms and perhaps even on the lower branch of chimney solutions, the flow in the mushy layer is driven by its own buoyancy and not principally by any suction from the chimney. Our results suggest that the changeover between the two sorts of behaviour described above is associated with the change between the chimney width first increasing and then decreasing with convective strength (figure 5d).

All the calculations displayed so far have been for $L = 2.16$, and we have found no steady solutions at this wavelength for $R_m < 11.1$. It is natural to ask whether finite-amplitude, steady solutions can exist, at other wavelengths, at lower Rayleigh numbers. In figure 7 we have plotted the linear critical Rayleigh number R_l and the global critical Rayleigh number R_g (shown on figure 5a), corresponding to the turning point of the branch of chimney solutions, as functions of L. We found that a minimum global critical Rayleigh number exists (which could not be found from the more approximate model of Schulze & Worster 1998) and that, for the parameters used here, it occurs at a slightly smaller wavelength than the linear critical wavelength. Though Loper & Roberts (2001) also predicted that chimneys can exist at subcritical Rayleigh numbers, the results following from their very different method of determining the chimney width have quite different characteristics: see figure 8, which can be contrasted with figures 5(b) and 5(d). In particular, Loper & Roberts predict that chimneys can exist at arbitrarily small values of R_m.

Recall that L is the dimensionless wavelength, scaled on the diffusion length which, for given material properties and far-field conditions, is proportional to the height of the mushy layer. Therefore, in a transient experiment in which the height of the mushy layer increases in time, the dimensionless spacing between two given chimneys

https://doi.org/10.1017/S0022112001007558 Published online by Cambridge University Press

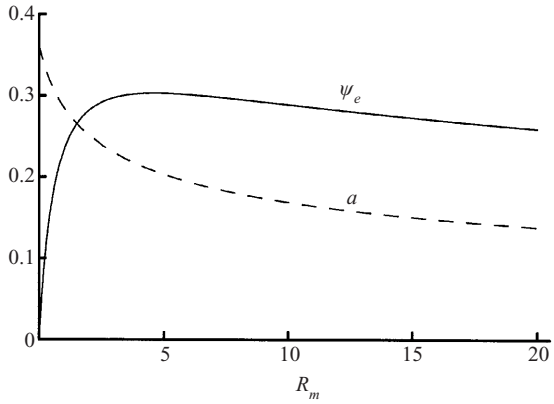


FIGURE 8. The constant width a of a chimney, and the dimensionless mass flux ψ_e emanating from it, predicted by Loper & Roberts (2001). The curves were calculated from their equations (115) and (128) using parameter values equal to those given in the caption to figure 3 and a Lewis number $L_e = \kappa/D = 100$, where D is the solutal diffusivity. Note that the analysis of Loper & Roberts is axisymmetric rather than two-dimensional and that here $\psi_e = (W^*/\kappa^{*2})Q_v^*$ in their notation.

decreases. Thus, as the layer grows, chimneys at a given physical spacing can reach a state below the global critical Rayleigh number and disappear. This behaviour has been seen in many laboratory experiments (see, for example Chen & Chen 1991; Chen, Yang & Lu 1993).

5. Liquid inclusions

As the strength of convection increases along the steady-solution branch bifurcating from the linear critical point, solutions can be found in which the solid fraction is zero within an interior region of the mushy layer (Schulze & Worster 1999). The upper boundary of such a liquid inclusion is a dissolving interface, and its location is determined by solute conservation (Worster 2002). Near the centreline, $x = 0$, the flow is from the liquid inclusion back into the mushy region, and solute conservation requires that

$$(\mathscr{C} - \theta)\phi(\boldsymbol{V} - \boldsymbol{V}_s)\cdot\boldsymbol{n} = \left[\theta - \Theta(\psi_q)\right]\boldsymbol{n}\cdot\boldsymbol{q}, \tag{5.1}$$

where $\boldsymbol{V}$ is the velocity of the mush–liquid interface, $\boldsymbol{V}_s$ is the velocity of the solid phase and $\boldsymbol{n}$ is the unit normal to the interface pointing into the mush. In the present system, this equation can be rewritten as

$$(\mathscr{C} - \theta)(a_t - a_z) = -\frac{\theta - \Theta(\psi_q)}{\phi}\left[\psi_z + (\psi_x - 1)a_z\right]. \tag{5.2}$$

This evolution equation clearly breaks down when $\phi = 0$, which corresponds to where $\boldsymbol{n}\cdot\boldsymbol{q} = 0$. There can exist a part of the dissolving interface (upper portion of the liquid inclusion) where the flow is from mush to liquid $\boldsymbol{n}\cdot\boldsymbol{q} < 0$. In this case, the interface is simply the locus of where $\phi = 0$. Therefore

$$(\boldsymbol{V} - \boldsymbol{V}_s)\cdot\boldsymbol{n} = \frac{-1}{\boldsymbol{n}\cdot\nabla\phi}\frac{\mathrm{D}^s\phi}{\mathrm{D}t} \tag{5.3}$$

at the interface, where $\mathrm{D}^s/\mathrm{D}t$ is a derivative following the solid phase. This equation

https://doi.org/10.1017/S0022112001007558 Published online by Cambridge University Press

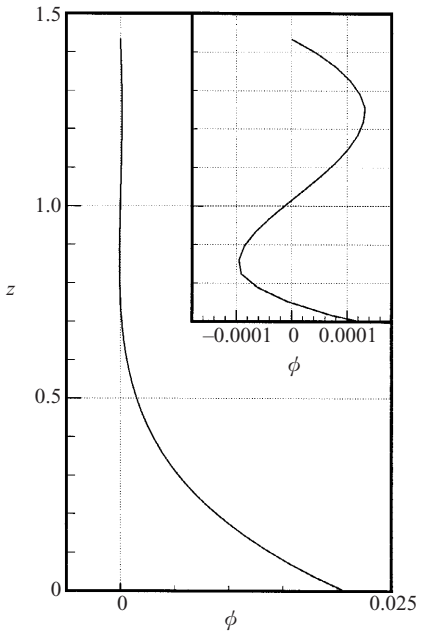


FIGURE 9. The solid fraction distribution just after the appearance of a region of negative solid fraction. The expanded horizontal scale used in the inset shows the small region of negative solid fraction (an incipient liquid inclusion) and the very small positive values of the solid fraction above it.

can be combined with the solute-conservation equation (2.2*b*) to give

$$(\mathscr{C}-\theta)(a_t-a_z)=\frac{\boldsymbol{q}\cdot\nabla\theta}{\phi_x}. \tag{5.4}$$

It is proved in Appendix A that the right-hand side of (5.2) is continuous with the right-hand side of (5.4) at the point where $\boldsymbol{n}\cdot\boldsymbol{q}=0$. In a numerical scheme, it is required that the expression for a_t be continuous all along the wall of the inclusion, the lower half of which is computed using (3.3*b*). We therefore propose the following scheme:

$$\frac{1}{\epsilon_2}\frac{\partial a}{\partial t}=\boldsymbol{q}\cdot\nabla\theta \quad \text{where} \quad a_z>0, \tag{5.5a}$$

$$\frac{1}{\epsilon_2}\frac{\partial a}{\partial t}=\boldsymbol{q}\cdot\nabla\theta+(\mathscr{C}-\theta)\phi_x a_z \quad \text{where} \quad a_z<0, \quad \boldsymbol{n}\cdot\boldsymbol{q}<0, \tag{5.5b}$$

$$\frac{1}{\epsilon_2}\frac{\partial a}{\partial t}=-\frac{\phi_x}{\phi}\left[\theta-\Theta(\psi_q)\right]\left[\psi_z+(\psi_x-1)a_z\right] +(\mathscr{C}-\theta)\phi_x a_z \quad \text{where} \quad a_z<0, \quad \boldsymbol{n}\cdot\boldsymbol{q}>0. \tag{5.5c}$$

Using these equations, the bottom of the inclusion occurs naturally at a stagnation point of $\boldsymbol{q}$ on the axis, similarly to the bottom of a fully developed chimney. The top of the inclusion occurs where

$$(\theta-\Theta_0)(\psi_x-1)=(\mathscr{C}-\theta)\phi, \tag{5.6}$$

i.e. where the vertical advection of solute-depleted liquid within the inclusion balances the release of solute by melting. We found (figure 9) that the solid fraction is extremely

https://doi.org/10.1017/S0022112001007558 Published online by Cambridge University Press

small above an incipient liquid inclusion, which would require a very small increase in the amplitude of convection in order to achieve the balance required by (5.6). Whether for this or other reasons, our numerical scheme seemed ill suited to converge to such solutions, though we believe that they should exist in principle.

6. Implications for a single-layer model

Significant computational effort is expended evaluating the flow in the liquid region. This is in part a consequence of the fact that, even while the mush Rayleigh number R_m is quite modest, the fluid Rayleigh number, characterizing the plume for example, is of order R_m/Da and can therefore be very large, given that $Da \ll 1$. Additionally, if solutal diffusion is retained then fine-scale convection can occur throughout the liquid region, originating from the boundary-layer mode of convection (Worster 1992). Often in the form of double-diffusive fingers (Tait & Jaupart 1989; Chen & Chen 1991), this fine-scale convection has been shown theoretically (Emms & Fowler 1994) to have little influence on the heat flux at the mush–liquid interface, and experimentally (Wettlaufer *et al.* 1997) to result in little solute transport. Therefore, flows in the liquid region can be vigorous and characterized by small length scales, requiring high-resolution numerical grids and small time steps. Yet resolving all this detail may be unnecessary to determine the main characteristics of the mushy layer, particularly the solute flux emanating from it.

Avoiding the solution of the liquid region has therefore been one of the principal simplifications sought in studies of solidification and convection of binary melts. By doing so, one can make the system mathematically tractable (for example, Fowler 1985; Amberg & Homsy 1993; Emms & Fowler 1994; Anderson & Worster 1995; Chung & Chen 2000*a*) or reduce the numerical difficulties (Schulze & Worster 1998; Chung & Chen 2000*b*). To achieve this goal without arbitrarily fixing the location of the mush–liquid interface, the values of the pressure and the temperature gradient along the mush–liquid interface must be prescribed in a way that mimics the transfers from the liquid region (see figure 2).

For example, Emms & Fowler (1994) showed that the pressure is uniform along the mush–liquid interface in the limit $Da \to 0$. Thus one can impose

$$p = 0 \quad (z = h(x)). \tag{6.1}$$

Additionally, Fowler (1985) solved a local, one-dimensional advection–diffusion problem for the thermal field in the liquid just above the mush–liquid interface to relate the heat flux to the far-field temperature and the flow from liquid to mush, in effect assuming that the thermal variations in the liquid are confined to a narrow boundary layer. We have extended this idea slightly, to take account of the curvature of the isotherms, and propose the condition

$$\boldsymbol{n} \cdot \nabla\theta = \theta_0[\nabla \cdot \boldsymbol{n} - \boldsymbol{n} \cdot \boldsymbol{q}] \quad (z = h(x)) \tag{6.2}$$

(see Appendix B). The curvature term, proportional to $\nabla \cdot \boldsymbol{n}$, we found necessary to limit the interface perturbation from growing unrealistically large at higher amplitudes of convection.

We have found that using constant pressure (6.1) in place of matching to the pressure in the liquid region causes only a 1% reduction in the linear critical Rayleigh number at $Da = 0.005$, whereas using (6.2) in addition causes a 12% reduction. If the curvature term is omitted from (6.2) then a 44% reduction in the critical Rayleigh

https://doi.org/10.1017/S0022112001007558 Published online by Cambridge University Press

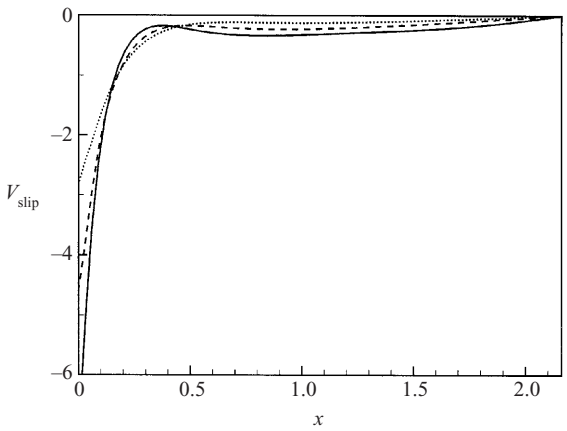


FIGURE 10. The slip velocities along the mush–liquid interface for $R_m = 12.9$: dotted curve $Da = 0.001$; dashed curve $Da = 0.003$; solid curve $Da = 0.01$.

number results. Overall, we have found that using (6.1) and (6.2) as boundary conditions in a single-layer model of a mushy layer gives reasonable quantitative predictions and good qualitative predictions of the subcritical bifurcation of convecting states prior to the formation of chimneys.

However, once a chimney forms, these boundary conditions are inadequate. The principal reason for this is that equation (6.1) does not allow any tangential component of flow in the mushy region at the mush–liquid interface. Given that the interface is an isotherm, tangential flow is required where the upper mush–liquid interface meets the chimney wall in order that equation (2.17) can be satisfied there. Our numerical computations of the full system suggest (figure 10) that, though equation (6.1) may be achieved pointwise as $Da \to 0$, the convergence is non-uniform and there is always a finite tangential velocity at $z = h(0)$. This can be explained as follows.

As buoyant fluid emerges from the chimney it accelerates rapidly, the magnitude of the acceleration increasing as the Darcy number decreases, given that the buoyancy term in (2.3*c*) is proportional to R_m/Da. This rapid acceleration turns the streamlines and causes low pressure near the vent of the chimney. The resulting pressure gradient in the vicinity of the vent drives a tangential flow along the interface. It may be possible to mimic this by a suitable modification of (6.1), for example by introducing an appropriate boundary layer around the chimney vent.

7. Summary and conclusions

We have analysed steady-state convection in a two-dimensional, solidifying system comprising a liquid region and a mushy region with periodically distributed chimneys. We have simultaneously determined the shapes of the mush–liquid interface and the chimney wall, which are both free boundaries within the system. The position of the chimney wall is determined locally at each height by a condition of equilibrium derived by Schulze & Worster (1999), which extends the physical reasoning originated by Loper & Roberts (2001) to identify the region of 'hidden mush' below a steady-state chimney.

Once a chimney forms, the morphology of the upper mush–liquid interface changes from being undular to being peaked at the chimney vent, as observed experimentally. The width of the chimney is predicted to be narrow compared with its length, its

https://doi.org/10.1017/S0022112001007558 Published online by Cambridge University Press

aspect ratio being roughly proportional to $Da^{1/3}$, where the Darcy number $Da \ll 1$ is the ratio of the permeability of the mushy layer to the square of the thermal diffusion length.

There is a short, subcritical branch of unstable convecting states with no chimneys bifurcating from a linear critical point, and a much larger branch of states with fully developed chimneys, the lower branch of which is unstable and the upper branch stable. We found that there is a minimum value of the Rayleigh number $R_m = \beta\Delta C g \Pi_0 / \nu V$ for which steady convection through chimneys can exist that is lower than the linear critical Rayleigh number and occurs at a slightly shorter wavelength. At a much higher Rayleigh number, we discovered a secondary convection cell, heralding an incipient chimney, which suggests that strongly convecting states will have chimneys spaced closer than the linear critical wavelength.

The dimensionless width of the chimney, scaled on the thermal diffusion length, first increases as the strength of convection increases causing more dissolution but ultimately decreases as the stronger inflow compresses the thermal boundary layer around the chimney. This latter trend is consistent with previous scaling analyses (Worster 1991; Schulze & Worster 1998) but our numerical results do not span a sufficient range to test the scaling relationships more precisely.

The branch of solutions with chimneys that we found is disconnected from the branch of convecting states with no chimneys. This gap should at least partially be filled with a branch of states in which there is an internal liquid inclusion (Schulze & Worster 1999, 2001), bifurcating from the branch of no chimneys. However, our numerical explorations, though inconclusive, suggest that there may be a range of Rayleigh numbers in which there are no steady solutions on the lower branch.

One of the principal aims of this research is the predictive determination of solute fluxes exchanged between mushy layers and the melts from which they grow. Some results regarding solute fluxes are given in figure 5(b) and the associated text but, because this study is two-dimensional, we are not yet in a position to make quantitative predictions that can be related to existing experimental or practical configurations. Nevertheless, the results of this paper do provide important indications of where and how solute fluxes are determined. For example, we have found that the solute that emerges from the chimneys is weighted towards that originating from nearer the mush–liquid interface. We have also found that, once chimneys are established, the overall flow is driven predominantly by the buoyancy within the chimneys, which therefore appear as sinks to the fluid in the surrounding mushy layer, each draining fluid from a horizontal domain of comparable width to the thickness of the layer. The most important point is that, because the internal dynamics of the chimneys control the overall flow (rather than the chimneys being a passive consequence of a flow driven by the buoyancy in the exterior mushy layer), the solute fluxes are sensitive to the width a of the chimneys, being proportional to the volume flux and therefore to a^3 in two dimensions and to a^4 in three dimensions. It is therefore imperative to obtain accurate predictions for the width of chimneys. This points to the need for high resolution of these narrow features in large-scale numerical computations, or to use the sort of hybrid analysis presented here, which exploits the scale separation to provide semi-analytical determinations of the fluxes within chimneys.

A fully analytical treatment of chimneys has been proposed by Loper & Roberts (2001). Their model and its results differ in significant ways from those proposed here. Loper & Roberts suggest that the width of a chimney is determined by conditions at its vent and that 'diffusion of material [i.e. solute diffusion] is essential in determining the chimney radius'. In contrast, we suggest that the width of a chimney is determined

https://doi.org/10.1017/S0022112001007558 Published online by Cambridge University Press

locally at each height by equilibrium thermodynamic constraints and have found solutions in the absence of solutal diffusion. Loper & Roberts predict that the chimney radius decreases to zero as the solute diffusion decreases to zero and that it decreases monotonically as the Rayleigh number R_m increases, having its largest value, therefore, at $R_m = 0$. Conversely, our model suggests that there is a critical Rayleigh number $R_m = R_g$ below which steady chimneys cannot exist.

In this paper we have established a new methodology with which to investigate steady convection through chimneys in a mushy layer. Our analysis was carried out using the equations for a two-dimensional, ideal mushy layer. The approach should readily extend to three dimensions and to calculations in which variable property values are used, which will be needed before quantitative comparisons with experimental results can be made. Using this method, we should soon be able to make simple predictions of macrosegregation in castings and of brine fluxes from sea ice, for example.

The authors would like to thank Falin Chen for providing a postdoctoral fellowship for C. A. C. from the National Science Council of Taiwan through Grant No. NSC 88-2212-E002-018. We benefitted from numerous discussions with Tim Schulze, and we are additionally grateful to him and to Falin Chen, Peter Guba, Herbert Huppert, Ross Kerr and John Wettlaufer for their helpful comments on a draft of the paper.

Appendix A. Continuity of evolution equations

Equations (5.1) and (5.3) govern the evolution of the ablating wall of a liquid inclusion, respectively where the flow is from liquid to mush and where it is from mush to liquid. These conditions are continuous with each other at the point where $\boldsymbol{n}\cdot\boldsymbol{q} = 0$. To see this it is necessary to show that

$$\frac{[\theta - \Theta(\psi_q)]\boldsymbol{n}\cdot\boldsymbol{q}}{\phi} \rightarrow \frac{\boldsymbol{q}\cdot\nabla\theta}{\boldsymbol{n}\cdot\nabla\phi} \tag{A 1}$$

at the transition point.

Note that all the dependent variables involved have continuous first derivatives, though not necessarily continuous second derivatives. Since the numerator and denominator of the left-hand side of (A 1) both tend to zero at the transition point, we can use L'Hopital's rule along a ray parallel to the flow vector $\boldsymbol{q}$ to show that

$$\frac{[\theta - \Theta(\psi_q)]\boldsymbol{n}\cdot\boldsymbol{q}}{\phi} \rightarrow \frac{\boldsymbol{q}\cdot\nabla[\theta - \Theta(\psi_q)]\boldsymbol{n}\cdot\boldsymbol{q}}{\boldsymbol{q}\cdot\nabla\phi} = \frac{(\boldsymbol{q}\cdot\nabla\theta)\boldsymbol{n}\cdot\boldsymbol{q}}{\boldsymbol{q}\cdot\nabla\phi} \tag{A 2}$$

since $\boldsymbol{q}\cdot\nabla\Theta = 0$ at the transition point, as it is everywhere on the liquid side of the interface. Now, it is also true that $\boldsymbol{t}\cdot\nabla\phi = 0$ at the transition point, where $\boldsymbol{t}$ is a vector tangent to the interface. Therefore $\nabla\phi$ is parallel to $\boldsymbol{n}$, so that $\nabla\phi = (\boldsymbol{n}\cdot\nabla\phi)\boldsymbol{n}$ and

$$\boldsymbol{q}\cdot\nabla\phi = \boldsymbol{q}\cdot(\boldsymbol{n}\cdot\nabla\phi)\boldsymbol{n} = \boldsymbol{n}\cdot\boldsymbol{q}\boldsymbol{n}\cdot\nabla\phi. \tag{A 3}$$

Using this expression in the denominator of (A 2), we obtain (A 1).

Appendix B. Approximate thermal boundary condition

When solutal diffusion is ignored, the top mush–liquid interface is an isotherm, as described in § 2. Let $\boldsymbol{n}$ and $\boldsymbol{t}$ be unit-vector fields that are everywhere respectively

https://doi.org/10.1017/S0022112001007558 Published online by Cambridge University Press

normal and tangential to isotherms. Then $\boldsymbol{t}\cdot\nabla\theta\equiv 0$ and

$$\nabla^2\theta=\nabla\cdot(\boldsymbol{n}\boldsymbol{n}\cdot\nabla\theta)=(\boldsymbol{n}\cdot\nabla)^2\theta+(\nabla\cdot\boldsymbol{n})\boldsymbol{n}\cdot\nabla\theta. \tag{B 1}$$

The thermal advection–diffusion equation in the liquid region (2.3a) can be written

$$\nabla^2\theta=\boldsymbol{q}\cdot\nabla\theta \tag{B 2}$$

$$\Rightarrow\frac{\partial^2\theta}{\partial n^2}+(\nabla\cdot\boldsymbol{n})\frac{\partial\theta}{\partial n}=(\boldsymbol{n}\cdot\boldsymbol{q})\frac{\partial\theta}{\partial n}, \tag{B 3}$$

where $\partial/\partial n\equiv\boldsymbol{n}\cdot\nabla$. The approximation consists in imagining that θ varies from its boundary value $\theta=0$ to its far-field value $\theta=\theta_0$ across a boundary layer in which the curvature of the isotherms $\nabla\cdot\boldsymbol{n}$ and the normal velocity $\boldsymbol{n}\cdot\boldsymbol{q}$ are treated as constant. Equation (B 3) can then be integrated across the boundary layer to give

$$\boldsymbol{n}\cdot\nabla\theta\big|_{n=0}=\theta_0[\nabla\cdot\boldsymbol{n}-\boldsymbol{n}\cdot\boldsymbol{q}], \tag{B 4}$$

which is equation (6.2).

Note that, for example, in a linear stability analysis, the linear velocity perturbation in the liquid region decays on the same scale as the critical wavelength, which is comparable to the thickness of the thermal boundary layer. Thus (B 4), by assuming that $\boldsymbol{n}\cdot\boldsymbol{q}$ is constant across the thermal boundary layer, over-estimates the perturbation to the heat flux and renders the system less stable.

REFERENCES

Amberg, G. & Homsy, G. M. 1993 Nonlinear analysis of buoyant convection in binary solidification with application to channel formation. *J. Fluid Mech.* **252**, 79–98.

Anderson, D. M. & Worster, M. G. 1995 Weakly nonlinear analysis of convection in a mushy layer during the solidification of binary alloys. *J. Fluid Mech.* **302**, 307–331.

Batchelor, G. K. 1967 *An Introduction to Fluid Dynamics*. Cambridge University Press.

Bergman, M. I. & Fearn, D. R. 1994 Chimneys on the Earth's inner-outer core boundary? *Geophys. Res. Lett.* **21**, 477–480.

Bergman, M. I., Fearn, D. R., Bloxham, J. & Shannon, M. C. 1997 Convection and channel formation in solidifying Pb–Sn alloys. *Metall. Mater. Trans.* **28A**, 859–866.

Chen, C. F. 1995 Experimental study of convection in a mushy layer during directional solidification. *J. Fluid Mech.* **293**, 81–98.

Chen, F. & Chen, C. F. 1991 Experimental study of directional solidification of aqueous ammonium chloride solution. *J. Fluid Mech.* **227**, 567–586.

Chen, F., Yang, T. L. & Lu, J. W. 1993 Influence of convection on solidification of binary solutions cooling from below. *J. Appl. Phys.* **74**, 7531–7541.

Chung, C. A. & Chen, F. 2000*a* Onset of plume convection in mushy layers. *J. Fluid Mech.* **408**, 53–82.

Chung, C. A. & Chen, F. 2000*b* Convection in directionally solidifying alloys under inclined rotation. *J. Fluid Mech.* **412**, 93–123.

Copley, S. M., Giamei, A. F., Johnson, S. M. & Hornbecker, M. F. 1970 The origin of freckles in unidirectionally solidified castings. *Metall. Trans.* **1**, 2193–2204.

Eide, L. I. & Martin, S. 1975 The formation of brine drainage features in young sea ice. *J. Glaciol.* **14** (70), 137–154.

Emms, P. W. & Fowler, A. C. 1994 Compositional convection in the solidification of binary alloys. *J. Fluid Mech.* **262**, 111–139.

Fearn, C. R., Loper, D. E. & Roberts, P. H. 1981 Structure of the Earth's inner core. *Nature* **292**, 232–233.

Felicelli, S. D., Heinrich, J. C. & Poirier, D. R. 1991 Simulation of freckles during vertical solidification of binary alloys. *Metall. Trans.* **22B**, 847–859.

Fowler, A. C. 1985 The formation of freckles in binary alloys. *IMA J. Appl. Maths* **35**, 159–174.

https://doi.org/10.1017/S0022112001007558 Published online by Cambridge University Press

Fowler, A. C. 1997 *Mathematical Models in the Applied Sciences*, pp. 318–323. Cambridge University Press.

Huppert, H. E. 1990 The fluid mechanics of solidification. *J. Fluid Mech.* **212**, 209–240.

Jellinek, A. M. & Kerr, R. C. 2001 Magma dynamics, crystallization and chemical differentiation of the 1959 Kilauea Iki lava lake, Hawaii, revisited. *J. Volcanol. Geotherm. Res.* **110**, 235–263.

Loper, D. E. 2001 On the boundary conditions at a mush–melt interface. *J. Cryst. Growth.* **222**, 655–666.

Loper, D. E. & Roberts, P. H. 2001 Mush–chimney convection. *Stud. Appl. Maths* **106**, 187–227.

Mullins, W. W. & Sekerka, R. F. 1964 Stability of a planar interface during solidification of a binary alloy. *J. Appl. Phys.* **35**, 444–451.

Press, W. H., Flannery, B. P., Teukolsky, S. A. & Vetterling, W. S. 1988 *Numerical Recipes*. Cambridge University Press.

Roberts, P. H. & Loper, D. E. 1983 Towards a theory of the structure and evolution of a dendrite layer. In *Stellar and Planetary Magnetism* (ed. A. M. Soward), pp. 329–349. Gordon & Breach.

Sample, A. K. & Hellawell, A. 1984 The mechanism of formation and prevention of channel segregation during alloy solidification. *Metall. Trans.* **15A**, 2163–2173.

Schneider, M. C., Gu, J. P., Beckermann, C., Boettinger, W. J. & Kattner, U. R. 1997 Modeling of micro- and macrosegregation and freckle formation in single-crystal nickel-base superalloy directional solidification. *Metall. Mater. Trans.* **28A**, 1517–1531.

Schulze, T. P. & Worster, M. G. 1998 A numerical investigation of steady convection in mushy layers during the directional solidification of binary alloys. *J. Fluid Mech.* **356**, 199–220.

Schulze, T. P. & Worster, M. G. 1999 Weak convection, liquid inclusions and the formation of chimneys in mushy layers. *J. Fluid Mech.* **388**, 197–215.

Schulze, T. P. & Worster, M. G. 2001 Mushy zones with fully developed chimneys. In *Interactive Dynamics of Convection and Solidification* (ed. P. Ehrhard, D. Riley & P. Steen). Kluwer.

Solomon, T. H. & Hartley, R. R. 1998 Measurements of the temperature field of the mushy and liquid regions during solidification of aqueous ammonium chloride. *J. Fluid Mech.* **358**, 87–106.

Tait, S., Jahrling, K. & Jaupart, C. 1992 The planform of compositional convection and chimney formation in a mushy layer. *Nature* **359**, 406–408.

Tait, S. & Jaupart, C. 1989 Compositional convection in viscous melts. *Nature* **338**, 571–574.

Tait, S. & Jaupart, C. 1992 Compositional convection in a reactive crystalline mush and melt differentiation. *J. Geophys. Res.* **97**, 6735–6759.

Wettlaufer, J. S., Worster, M. G. & Huppert, H. E. 1997 Natural convection during solidification of an alloy from above with application to the evolution of sea ice. *J. Fluid Mech.* **344**, 291–316.

Wettlaufer, J. S., Worster, M. G. & Huppert, H. E. 2000 The solidification of leads: theory, experiment and field observations. *J. Geophys. Res.* **105**, 1123–1134.

Worster, M. G. 1991 Natural convection in a mushy layer. *J. Fluid Mech.* **224**, 335–359.

Worster, M. G. 1992 Instabilities of the liquid and mushy regions during solidification of alloys. *J. Fluid Mech.* **237**, 649–669.

Worster, M. G. 1997 Convection in mushy layers. *Annu. Rev. Fluid Mech.* **29**, 91–122.

Worster, M. G. 2000 Solidification of Fluids. In *Perspectives in Fluid Dynamics: a Collective Introduction to Current Research* (ed. G. K. Batchelor, H. K. Moffatt & M. G. Worster), pp. 393–446. Cambridge University Press.

Worster, M. G. 2002 Interfaces on all scales during solidification and melting. In *Interfaces for the 21st Century* (ed. M. K. Smith, M. J. Miksis, G. P. Neitzel, G. B. McFadden & D. R. Canright) (in press).

https://doi.org/10.1017/S0022112001007558 Published online by Cambridge University Press